ACS APPLIED MATERIALS & INTERFACES

Letter

www.acsami.org

Order−Disorder Transition in the Molecular Orientation during Initial Growth of Organic Thin Film

Soonnam Kwon,[†,‡] Tae Gun Kim,[§] Won Kook Choi,[‡] Sang Ook Kang,*[,†] and Jeong Won Kim*[,§]

[†]Department of Advanced Materials Chemistry, Korea University, 2511 Sejong-ro, Sejong 339-700, South Korea

[§]Korea Research Institute of Standards and Science, 267 Gajeong-ro, Daejeon 305-340, South Korea

[‡]Interface Control Research Center, Future Convergence Research Division, Korea Institute of Science and Technology, Hwarangno 14 gil 5, Seoul, 136-791 Korea

Supporting Information

ABSTRACT: We report on the identification of molecular orientation and its order−disorder transition during the initial growth of 1,3-bis(N-carbazolyl)benzene (mCP) thin films on a highly ordered pyrolytic graphite (HOPG) surface by using photoelectron spectroscopy (PES). Theoretical PES amplitudes using a quantum mechanical calculation that adapts independent atomic center approximation (IAC) were calculated to compare with experimental observations. At low coverage, an equilibrium orientation of isolated adsorbate was estimated. As the coverage increases, the interaction between adsorbates becomes dominant and raises the disorder, which results in changes in the PES shapes as well as the line broadening of each peak.

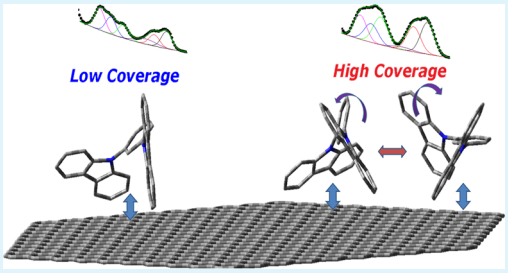

KEYWORDS: *photoelectron spectroscopy, quantum mechanical calculation, order−disorder transition, molecular orientation*

1. INTRODUCTION

Understanding the molecular geometry at (in)organic/organic interfaces is one of prerequisites to investigate the electronic properties of organic devices. That is because the energy level alignment and the dynamics in charge carrier transfer strongly depend on the distance and orientation of constituent molecules relative to the interface.[1−3] There are several different methods that have been used to probe an interfacial molecular geometry, including STM,[4] grazing ellipsometry,[5] X-ray scattering,[6−11] and solid-state NMR.[12] In particular, X-ray scattering or diffraction has widely been utilized to see an organic film growth and geometrical transition under various growth condition.[6−11] However, this is limited to rather simple molecules in homogeneous state. Photoelectron spectroscopy (PES) has also been utilized as a tool for the determination of molecular geometry as well as electronic structural studies.[13−15] The fundamental advantage of the PES over other methods is that it can easily control interfacial sensitivity when it is combined with in situ film deposition.

Over the last few decades, several research groups have pioneered using PES as a tool for the identification of molecular orientation on various substrates with or without ordering.[16,17] A distinct PES peak shape is basically due to different photoionization cross sections for different energy states, which vary according to the order of molecular orientation on a substrate.[15] The gradual change in PES shape triggered by the increase in population of adsorbate molecules implies local order or disorder as a result of interaction between them. This type of study regarding order and disorder transition during adsorption on a substrate has long been an important problem in the area of surface science. The details of molecular geometries vary with deposition procedure or its coverage.[18] However, previous approaches have been limited mainly to planar molecules and well-defined equilibrium systems. Thus, tracing a nonplanar molecular geometry as a function of coverage still remains a challenging task.

In this study, the work by Ueno et al.[15] is generalized to a three-dimensional molecule, 1,3-bis(N-carbazolyl)benzene (mCP) which is a widely used host material for phosphorescent organic light-emitting diodes. The two carbazole (Cz) units are linked at the meta-position of a phenyl ring, which enables wide band gap and high charge carrier mobility.[19] Quantum mechanical calculation utilizing the independent atomic center (IAC) approximation is conducted to determine the equilibrium orientation of an adsorbate at low coverage, by comparing the calculated PES spectrum with an experimental one.[14] As the coverage increases, the relative intensity ratio changes and spectral line width increases. To explain the former under high coverage, simplified models which consist of various ensembles of disordered single molecules are introduced. Based on these disordered ensembles, we have successfully explained the experimental change in the PES shape from the calculation of statistical PES spectra. These phenomena are interpreted to be due to the adsorbate−adsorbate interaction at higher

Received: December 30, 2012
Accepted: March 4, 2013
Published: March 4, 2013

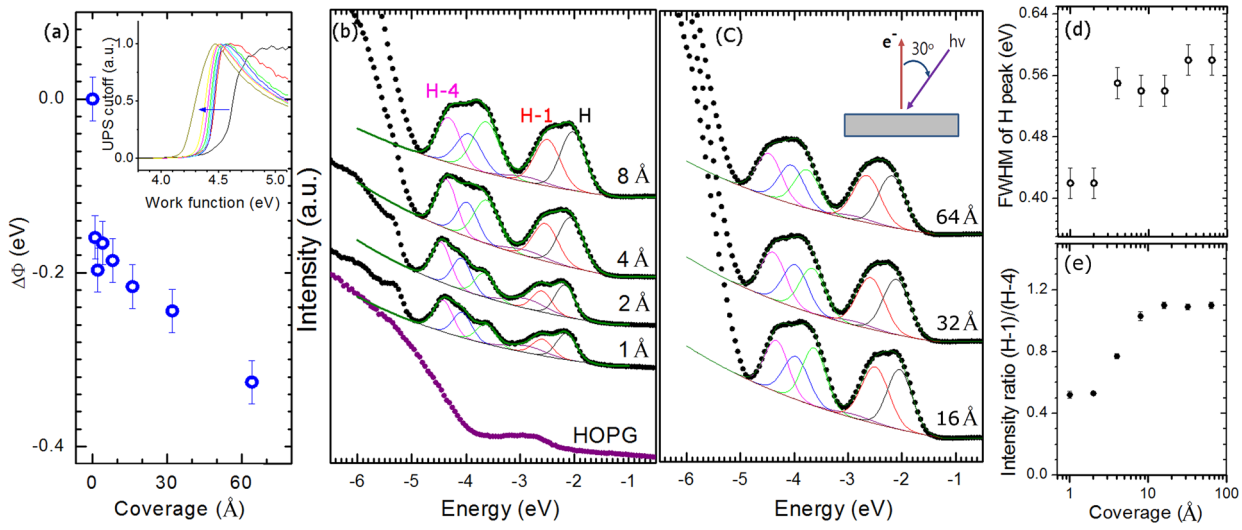

Figure 1. (a) Coverage-dependent work function change of mCP on HOPG. Inset: Secondary electron cutoffs as a function of coverage of mCP. (b, c) Frontier valence regions of PES spectra are shown as a function of coverage obtained from normal emission (NE) geometry, in which inset defines the measurement geometry. Circles represent experimental data and lines are the results of convolution. The violet curves at around −3 eV are from the underlying HOPG. (d) fwhm curves of convoluted H peaks in b and c as a function of coverage. (e) Intensity ratios of convoluted H-1 with respect to H-4 are shown as a function of coverage.

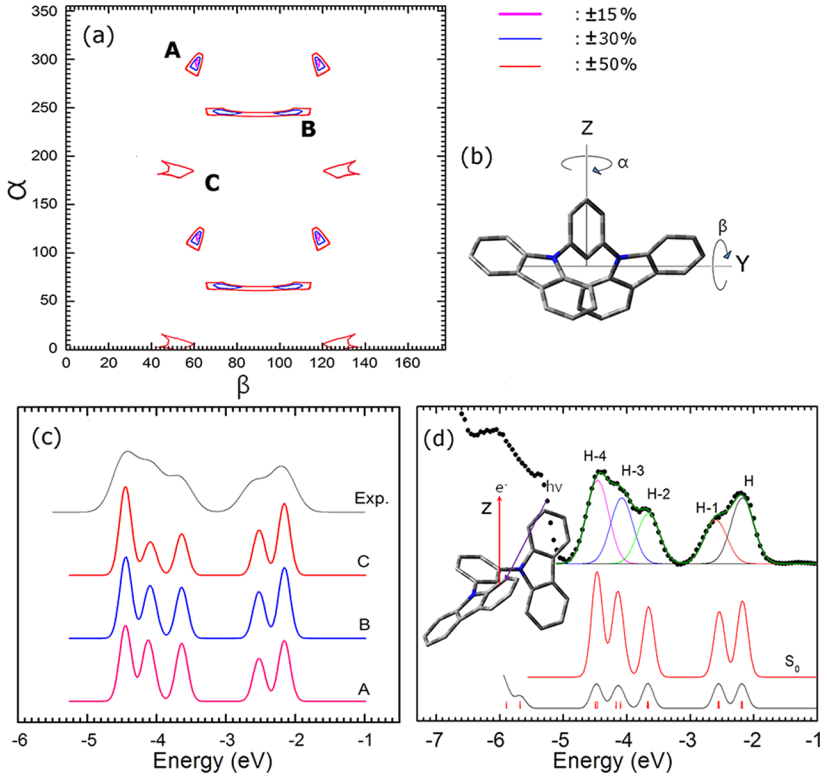

Figure 2. (a) Contour map of percent error of calculated intensity as a function of Euler rotation angles (α and β), which are defined in (b). (c) Comparison of the simulated PES signals for the molecular geometric regions, A, B, and C. (d) Background subtracted PES spectrum is compared with simulated spectra of mCP molecule with (red) and without (black) corrections for PES cross section. Insets: one example of possible molecular orientation (S_0), in which z axis is surface normal.

coverages. Thus, the order and disorder transition in three-dimensional molecular orientation during molecular growth is elaborated on. This explanation is also in agreement with the observation of increased line width of each peak, which can also be related to the change of polarization energy[20] or energy splitting due to intermolecular interaction.[21,22]

2. EXPERIMENTAL SECTION

The mCP films were deposited on HOPG substrate (ZYA-grade) at room temperature by thermal evaporation at pressures less than 6.7×10^{-6} Pa, with a deposition rate of 0.1 Å/s, which was measured with a calibrated quartz crystal microbalance. The substrate HOPG had been thoroughly outgassed by maintaining it at 573 K overnight. Spectral

Table 1. Relative Intensities of Experimental (I_{exp}) and Calculated (I_{cal}) Peaks with Respect to That of H-4

	H-3	H-2	H-1	H
I_{exp}[a]	0.79 ± 0.018	0.60 ± 0.014	0.53 ± 0.012	0.79 ± 0.018
I_{cal}[b]	0.85	0.66	0.61	0.72
error[c] (%)	−8	−10	−16	+9

[a]Intensity ratios (I/I_{H-4}) obtained from 2 Å spectrum in Figure 2d. [b]Intensity ratios (I/I_{H-4}) obtained from calculated PES at the S_0 geometry. [c]Error percentage = $[(I_{exp} - I_{cal})/I_{exp}] \times 100$.

measurements were performed in an UHV system by using a hemispherical electron energy analyzer (SES-100, VG-Scienta) with an unpolarized He I (21.2 eV) gas discharge lamp.[23] The light incidence and electron emission angles were 30° and 0°, respectively, for normal emission. The samples were biased at −10 V for work-function measurements. The atomic coordinates of mCP were obtained by X-ray structure data,[24] refined by geometry optimization using the B3LYP/6-31G-(D,P) level of theory on the platform of Gaussian 09 package.[25] Simulation of PES was performed using a conventional method, in which each Kohn−Sham (K−S) energy level is considered as having Gaussian distribution with full width at half-maximum (fwhm) of 0.2 eV.[3,21]

3. RESULTS AND DISCUSSION

In Figure 1a, the work function of HOPG exhibits a fast drop from 4.62 to 4.47 eV upon 1 Å of mCP deposition. From 2 to 8 Å, the work function change is marginal, and it decreases steadily until 64 Å, which indicates an incomplete coating of the mCP thin film. In panels b and c in Figure 1, valence electronic structures are shown. The signal-to-background ratio increases as the molecular thickness increases. Until 2 Å, no significant changes are observed, which indicates no interaction between adsorbates up to this coverage. However, from 4 Å, the shapes of spectra show remarkable changes, exhibiting saturation at 64 Å. In fact, the 64 Å spectrum shows no significant features on the overall shape and exhibits apparently similar intensity for all the energy states.

During the convolution process in panels b and c in Figure 1, base lines are assumed to consist of an exponential curve, which originates from secondary electrons, and a Gaussian curve, which is ascribed to the underlying HOPG around −2.9 eV. When choosing the convolution parameters, we tried to minimize the intensities at −5.0 and −3.1 eV, because these points are expected to be in the energy-level deficient regions, which is evident from the result of DFT calculation as shown in Figure 2. The details of the convolution process are given in the Supporting Information.

The most outstanding characteristics of the spectra at low coverage are the relatively narrow line width (0.42 eV) and well-distinguished intensity difference between energy states: at low coverage, H-4 shows the largest intensity, while H-1 exhibits the lowest value. When the thickness increases to 4 and 8 Å, the clear difference in the intensity becomes mitigated, resulting in a completely different overall shape of the PES spectra. This is evident if the intensity ratios (H-1)/(H-4) are monitored as a function of coverage as shown in Figure 1e. The intensity ratio shows marginal change until 2 Å (0.53), starts to increase from 4 Å, and saturates to 1.1 at 64 Å. In Figure 1d, the changes in the line width of H are shown as a function of coverage. fwhm of H increases from 0.42 to 0.55 eV as the coverage increases from 2 to 4 Å, which is apparently abrupt.

In Figure 2d, UPS spectrum at 2 Å after background and HOPG signal subtraction is shown. The bottom curves indicate the calculated K−S energy levels and simulated UPS of a single mCP molecule, respectively. The first ten frontier occupied K−S energy levels are doubly degenerated due to two equivalent Cz units attached to a phenyl in mCP. For convenience, the degenerate energy states are designated as H, H-1, H-2, H-3, and H-4. The position of each energy state can be assigned to the five experimental peaks on the 2 Å PES spectrum. Each peak of the experimental spectrum clearly shows different relative intensity, as summarized in Table 1. H-1 state shows the most intriguing behavior in that it has the lowest intensity compared to the others.

The intensity difference on a spectrum can be ascribed to the different PES cross sections, which depend on initial energy state of a molecule.[13−15] Following mostly the works of Hasegawa et al., (details in the Supporting Information) and taking into account the effect of unpolarized light source, the calculations of the PES cross section were averaged over all the possible linear polarizations of incident light. To reflect the effects of the azimuthal disorder of HOPG due to its micrograin structure, the calculations were also averaged over the substrate azimuthal angles.[15] To determine the molecular orientation that can account for the experiment, all the possible geometries were examined by rotating a molecule according to the following formula

$$\begin{pmatrix} x \\ y \\ z \end{pmatrix} = \hat{S}_i \begin{pmatrix} x' \\ y' \\ z' \end{pmatrix} = R_y(\beta) R_z(\alpha) \begin{pmatrix} x' \\ y' \\ z' \end{pmatrix} \quad (1)$$

for which the rotations, α and β, are defined in Figure 2b. There are only two nontrivial Euler angles, because the azimuthal angle, γ, is averaged in the calculation of PES cross section as mentioned above. The atomic orbital coefficients were then obtained using modified neglect of diatomic overlap (MNDO) calculation based on the rotated coordinates. Taking the above coefficients and the rotated coordinates, PES cross sections from each energy state were calculated (see Figure S2 in the Supporting Information)[15] for the specified detection geometry. From these PES cross sections, a weighted simulation of PES is obtained by multiplying the amplitude of each K−S energy level by the corresponding PES cross section. The intensity ratios of each representative energy state with respect to that of H-4 are plotted as a function of orientations (see Figure S3 in the Supporting Information). It results in the most probable molecular orientation, where the calculated intensity ratios best mimic those of experimental ones. Figure 2a illustrates three plausible regions with different errors ranging up to ±50%. Even if considering a large error tolerance of ±50%, the corresponding areas for Euler angles are very small. This indicates that the PES amplitude of each energy state is sensitive to the molecular orientation. In Figure 2c, three different regions, A-C produce completely different spectral weights. Thus, one can examine correct molecular orientation in more detail by comparing the experimental spectrum over

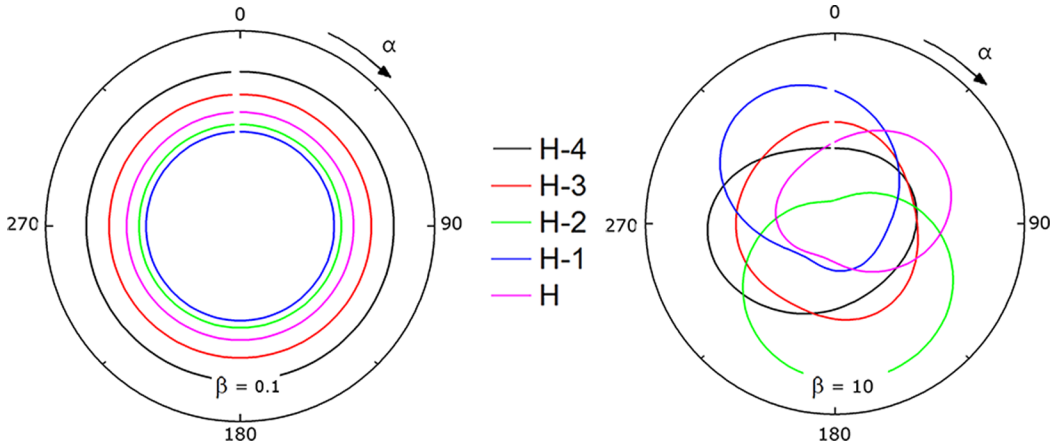

Figure 3. Comparison of intensities of the representative five energy states on the simulated PES based on the disordered noncumulative ensembles as a function of α angle. Radius represents intensity. Angles, α and β are defined in Figure 2b. All of the disorders are defined with respect to S_0.

the narrow regions in Figure 2a. The purple contours represent the regions, in which calculation and experiment coincide within an estimated error of ±15%. With higher accuracy, the area would be reduced further. In this way, molecular geometries within a specific range of errors were found, and one representative orientation (S_0) is shown in the inset of Figure 2d (see Figure S4 in the Supporting Information). The red curve represents the weighted simulation of PES for the S_0. The resulting intensity ratios obtained by the calculation and measurement are listed in Table 1, denoted as I_{cal} and I_{exp}, respectively. Thus, the current experimental PES features match the specific molecular orientation S_0 remarkably well. One might imagine that molecules on HOPG do not have any molecular order. However, the above results indicate that the landing molecules have a stable orientation, in which the binding energy with the substrate possesses a local minimum point (see Figure S5 in the Supporting Information). Nonetheless, because of the sensitivity of the binding energy between adsorbates and substrate, such a stationary orientation might have dependence on the thin film preparation condition and the surface treatment.

Finally, we discuss the implication of the errors between experiment and calculation, in which the errors cannot be reduced to zero. In the case of S_0, maximum error is −16% for the peak H-1. The origin of the limitation can be ascribed to the following causes. First, the orientation of mCP may not have a fixed one, but have slight disorder around a stationary orientation, S_0. Second, the molecule itself may suffer from disruption in geometric conformation due to interaction with substrate. Third, the approximation (IAC) used in the calculation may have posed the limitation in accuracy.

Now we turn our attention to the spectra above 4 Å coverage, in which the overall PES intensities gradually become similar to each other. For systematic investigation of the molecular structures at high coverage, a statistical ensemble of single molecules with disordered orientation around S_0 was generated as follows

$$\Omega = \Omega(\hat{S}_1 S_0, \ldots \hat{S}_i S_0, \ldots \hat{S}_N S_0) \tag{2}$$

where $\hat{S}_i$ represents the rotation transform matrix of the ith molecule in an ensemble as defined in eq 1. The PES cross-section of the nth energy state from the molecules in this ensemble can be obtained by the ensemble average using the following formula

$$\langle A_n(\vec{R})\rangle_\Omega = \frac{1}{N}\sum_{i=1}^{N} A_n(\vec{R}, \hat{S}_i S_0) \tag{3}$$

where $A_n(\vec{R}, \hat{S}_i S_0)$ represents the contribution from the ith molecule in the ensemble, and $\vec{R}$ represents the detector position. Two kinds of disordered ensembles were generated: (i) with β angles fixed to a nonzero value and 100 equally spaced α angles included. And (ii) with 250 randomly selected orientations with β angles less than a specified value, which is called a cumulative ensemble. In the cumulative ensemble, the ensemble number 250 was chosen, because this number was the minimum number to guarantee the reproducibility in the random selection. Figure 3 illustrates the effect of disorder in α angle at a fixed β angle in a noncumulative ensemble on the intensity of the weighted simulation of PES. For negligibly small β, the intensity changes are negligible. But as the disorder in β increases, the relative intensity strongly depends on α. Averaging each ensemble over α, the intensity difference becomes gradually vague.

Figure 4 illustrates the ensemble averaged relative intensity ratios, (H-1)/(H-4), as a function of disorder parameter. In case of noncumulative ensembles, the ratio (blue triangle) becomes unity around 12° and approaches a maximum at 30°, a minimum at 60°, and finally assumes a value of 0.93 at 90°. The curve shows mirror symmetry with respect to 90°. The noncumulative ensemble shows obvious dependence of the intensity ratio on the β deviation, but this oscillatory behavior is related to a disorder deviated from the S_0 rather than a random disorder. In the case of a cumulative ensemble, the ratio (black squares) shows damping oscillator-like behaviors, in which the ratio shows initial monotonic increase with maximum value of 1.57 at 40° and finally approaching around 1.15 by 150° because of random distribution of β in the cumulative ensemble. The intensity ratios for other energy states also showed similar damping oscillator-like behaviors, converging to values between 1.0 and 1.1. Cumulative ensembles represent completely random disorder within a given value of β. Even though these simulate nicely the initial changes of PES intensities, care should be paid when we correlate these to the experimental PES, because the molecules in real thin film may not be completely random, but have a limited level of order.[21] Nevertheless, we can obtain qualitative understanding on the peculiar changes in the overall shapes of PES spectra as a function of coverage. As the coverage increases, the adsorbate–

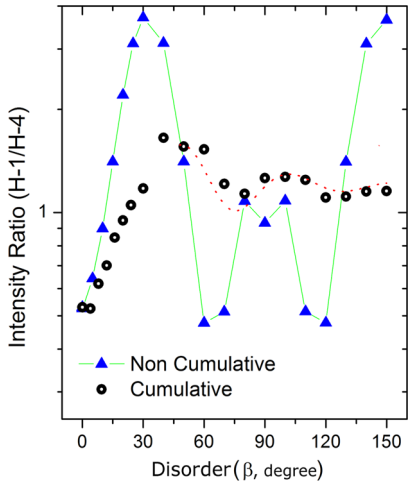

Figure 4. Intensity ratios of H-1 to H-4 obtained from the simulated PES, which was calculated from the ensemble of single molecules with a disorder in orientation from the suggested orientation, S_0. Each point is obtained by the average on each ensemble represented by disorder parameter, β. Red dots represent mathematical damping oscillator curve for guide to eyes.

substrate interaction is supposed to be disturbed by interactions between adsorbates. Such a weak van der Waals type interaction takes place in quite a random manner, which rationally brings out disorder in the molecular orientation, particularly for the nonplanar molecules like mCP.

In this reasoning, any detailed interaction between adsorbates was not considered due to the complexity involved in the interaction.[21] Nevertheless, there is another clue to the intermolecular interactions, which is the abrupt increase in line width of each peak, as shown in Figure 1d. Apart from hole-vibration coupling or crystalline band effect, the position and width of molecular orbital features on PES reflect inter- or intramolecular interaction.[26−28] Such mixed environments give rise to inhomogeneous molecular geometries, which can be related to either inhomogeneous distribution of polarization energy effect,[20] or energy splitting of the previously degenerated states.[21,22] Both effects together with hole-vibration effects[28] contribute to the line width of PES under study. In any case, the significant increase in line width of the H peak is basically originated from intermolecular interaction.

4. CONCLUSIONS

In conclusion, we have compared experimental PES spectra with a simulated one by using quantum mechanical calculations with IAC approximation. This method provides systematic estimation of molecular orientation and disorder, even for nontrivially shaped molecules. At low coverage of mCP adsorbates, they show a preferential orientation on the HOPG substrate. However, as the coverage increases, they interact with each other predominantly, and produce considerable disorder in the molecular orientation. This work does not only reveal an unprecedented way to interpret the adsorption behavior of weakly interacting system without long-range order, but also provides interface structural information of a useful molecule in organic electronics.

■ ASSOCIATED CONTENT

Supporting Information

Additional procedures for experimental data fitting, IAC approximation to three-dimensional molecules, and determination of equilibrium molecular orientation. This information is available free of charge via the Internet at http://pubs.acs.org/.

■ AUTHOR INFORMATION

Corresponding Author

*E-mail: sangok@korea.ac.kr (S.O.K.); jeongwonk@krisst.re.kr (J.W.K.).

Notes

The authors declare no competing financial interest.

■ ACKNOWLEDGMENTS

This work was supported by the Industrial strategic technology development program (10041556) funded by the Ministry of Knowledge Economy (MKE, Korea) and a research project of the National Research Foundation of Korea (Grant 2012-0006893).

■ REFERENCES

(1) Ishii, H.; Sugiyama, K.; Ito, E.; Seki, K. *Adv. Mater.* **1999**, *11*, 605−625.
(2) Hosokai, T.; Machida, H.; Gerlach, A.; Kera, S.; Schreiber, F.; Ueno, N. *Phys. Rev. B* **2011**, *83*, 195310.
(3) Brédas, J.-L.; Beljonne, D.; Coropceanu, V.; Cornil, J. *Chem. Rev.* **2004**, *104*, 4971−5004.
(4) Stadtmüller, B.; Sueyoshi, T.; Kichin, G.; Kröger, I.; Soubatch, S.; Temirov, R.; Tautz, F. S.; Kumpf, C. *Phys. Rev. Lett.* **2012**, *108*, 106103.
(5) Yokoyama, D.; Sakaguchi, A.; Suzuki, M.; Adachi, C. *Appl. Phys. Lett.* **2008**, *93*, 173302−173303.
(6) Zegenhagen, J. *Surf. Sci. Rep.* **1993**, *18*, 202−271.
(7) Gerlach, A.; Hosokai, T.; Duhm, S.; Kera, S.; Hofmann, O. T.; Zojer, E.; Zegenhagen, J.; Schreiber, F. *Phys. Rev. Lett.* **2011**, *106*, 156102.
(8) Fenter, P.; Schreiber, F.; Zhou, L.; Eisenberger, P.; Forrest, S. R. *Phys. Rev. B* **1997**, *56*, 3046−3053.
(9) Ruiz, R.; Choudhary, D.; Nickel, B.; Toccoli, T.; Chang, K.-C.; Mayer, A. C.; Clancy, P.; Blakely, J. M.; Headrick, R. L.; Iannotta, S.; Malliaras, G. G. *Chem. Mater.* **2004**, *16*, 4497−4508.
(10) Hong, S.; Amassian, A.; Woll, A. R.; Bhargava, S.; Ferguson, J. D.; Malliaras, G. G.; Brock, J. D.; Engstrom, J. R. *Appl. Phys. Lett.* **2008**, *92*, 253304−253303.
(11) Kowarik, S.; Gerlach, A.; Schreiber, F. *J. Phys.: Condens. Matter* **2008**, *20*, 184005.
(12) Neyshtadt, S.; Jahnke, J. P.; Messinger, R. J.; Rawal, A.; Segal Peretz, T.; Huppert, D.; Chmelka, B. F.; Frey, G. L. *J. Am. Chem. Soc.* **2011**, *133*, 10119−10133.
(13) Liebsch, A. *Phys. Rev. B* **1976**, *13*, 544−555.
(14) Grobman, W. D. *Phys. Rev. B* **1978**, *17*, 4573−4585.
(15) Hasegawa, S.; Tanaka, S.; Yamashita, Y.; Inokuchi, H.; Fujimoto, H.; Kamiya, K.; Seki, K.; Ueno, N. *Phys. Rev. B* **1993**, *48*, 2596−2600.
(16) Höfer, U.; Breitschafter, M. J.; Umbach, E. *Phys. Rev. Lett.* **1990**, *64*, 3050−3053.
(17) Puschnig, P.; Reinisch, E. M.; Ules, T.; Koller, G.; Soubatch, S.; Ostler, M.; Romaner, L.; Tautz, F. S.; Ambrosch-Draxl, C.; Ramsey, M. G. *Phys. Rev. B* **2011**, *84*, 235427.
(18) Hänel, K.; Söhnchen, S.; Lukas, S.; Beernink, G.; Birkner, A.; Strunskus, T.; Witte, G.; Wöll, C. *J. Mater. Res.* **2004**, *19*, 2049−2056.
(19) Adamovich, V.; Brooks, J.; Tamayo, A.; Alexander, A. M.; Djurovich, P. I.; D'Andrade, B. W.; Adachi, C.; Forrest, S. R.; Thompson, M. E. *New J. Chem.* **2002**, *26*, 1171−1178.
(20) Salaneck, W. R. *Phys. Rev. Lett.* **1978**, *40*, 60−63.

(21) Kwon, S.; Wee, K.-R.; Kim, J. W.; Pac, C.; Kang, S. O. *J. Chem. Phys.* **2012**, *136*, 204706−204708.
(22) Kera, S.; Fukagawa, H.; Kataoka, T.; Hosoumi, S.; Yamane, H.; Ueno, N. *Phys. Rev. B* **2007**, *75*, 121305.
(23) Kim, Y. H.; Kwon, S.; Lee, J. H.; Park, S. M.; Lee, Y. M.; Kim, J. W. *J. Phys. Chem. C* **2011**, *115*, 6599−6604.
(24) Han, W.-S.; Son, H.-J.; Wee, K.-R.; Min, K.-T.; Kwon, S.; Suh, I.-H.; Choi, S.-H.; Jung, D. H.; Kang, S. O. *J. Phys. Chem. C* **2009**, *113*, 19686−19693.
(25) Frisch, M. J.; Trucks, G. W.; Schlegel, H. B.; Scuseria, G. E.; Robb, M. A.; Cheeseman, J. R.; Scalmani, G.; Barone, V.; Mennucci, B.; Petersson, G. A.; Nakatsuji, H.; Caricato, M.; X. Li, H. P. H.; Izmaylov, A. F.; J. Bloino, G. Z., Sonnenberg, J. L.; Hada, M.; Ehara, M.; Toyota, K.; Fukuda, R.; Hasegawa, J.; Ishida, M.; Nakajima, T.; Honda, Y.; Kitao, O.; Nakai, H.; Vreven, T.; Montgomery, J. A.; , Jr., Peralta, J. E.; Ogliaro, F.; Bearpark, M.; Heyd, J. J.; Brothers, E.; Kudin, K. N.; Staroverov, V. N.; Kobayashi, R.; Normand, J.; Raghavachari, K.; Rendell, A.; Burant, J. C.; Iyengar, S. S.; Tomasi, J.; Cossi, M.; Rega, N.; Millam, J. M.; Klene, M.; Knox, J. E.; Cross, J. B.; Bakken, V.; Adamo, C.; Jaramillo, J.; Gomperts, R.; Stratmann, R. E.; Yazyev, O.; Austin, A. J.; Cammi, R.; Pomelli, C.; Ochterski, J. W.; Martin, R. L.; Morokuma, K.; Zakrzewski, V. G.; Voth, G. A.; Salvador, P.; Dannenberg, J. J.; Dapprich, S.; Daniels, A. D.; Ö. Farkas, Foresman, J. B.; Ortiz, J. V.; Cioslowski, J.; Fox, D. J. *GAUSSIAN*, revision A.02 ed.; Gaussian Inc.: Wallingford, CT, 2009.
(26) Kera, S.; Yamane, H.; Ueno, N. *Prog. Surf. Sci.* **2009**, *84*, 135−154.
(27) Krause, S.; Casu, M. B.; Schöll, A.; Umbach, E. *New J. Phys.* **2008**, *10*, 085001.
(28) Yamane, H.; Nagamatsu, S.; Fukagawa, H.; Kera, S.; Friedlein, R.; Okudaira, K. K.; Ueno, N. *Phys. Rev. B* **2005**, *72*, 153412.